Quaternary International 601 (2021) 15–27

Contents lists available at ScienceDirect

Quaternary International

journal homepage: www.elsevier.com/locate/quaint

A multi-proxy reconstruction of depositional environment of a Late Pleistocene submerged site from the Central Coast of Chile (32°): Implications for drowned sites

Valentina Flores-Aqueveque [a,b,c,*], Cristina Ortega [d], Rodrigo Fernández [a], Diego Carabias [b,e], Renato Simonetti [b,e], Isabel Cartajena [b,f], Laura Díaz [g], Charles González [a]

[a] Departamento de Geología, Facultad de Ciencias Físicas y Matemáticas, Universidad de Chile, Santiago, Chile
[b] ARQMAR-Centre for Maritime Archaeology Research of the Southeastern Pacific, Valparaíso, Chile
[c] Millennium Nucleus Paleoclimate, ANID Millennium Science Initiative, Santiago, Chile
[d] Escuela de Ingeniería, Facultad de Ingeniería y Arquitectura, Universidad Central de Chile, Santiago, Chile
[e] ÀRKA – Maritime Archaeology, Valparaíso, Chile
[f] Departamento de Antropología, Facultad de Ciencias Sociales, Universidad de Chile, Santiago, Chile
[g] Departamento de Ciencias Geológicas, Facultad de Ingeniería y Ciencias Geológicas, Universidad Católica Del Norte, Antofagasta, Chile

ARTICLE INFO

Keywords:
Submerged landscape
Last glacial maximum
South America
Sedimentary environment

ABSTRACT

Site GNL Quintero 1 (GNLQ1), located on the central Chilean coast (32°S), remains the only submerged fini-Pleistocene landscape reported for the southeastern Pacific coast to date. This unique site is characterized by a high frequency and diversity of extinct terrestrial faunal remains supported within a fine-grained sedimentary matrix. Several studies have been performed on the faunal assemblage; however, the sedimentary environment in which the site was formed still remains unclear. In this work, stratigraphic, sedimentological and geochemical analyses conducted on two marine cores are combined with seismic data to determine the depositional conditions affecting the formation of this exceptional shallowly buried submerged landscape. Previous results indicated that site GNLQ1 formed, at least between 28 and 21 ka, in an aquifer-fed freshwater lagoon that developed on a fluvial plain. Here, we show a three-stage sedimentological evolution. In the first stage, a shallow restricted freshwater lagoon formed under relatively arid conditions. Subsequently, the lagoon expanded and deepened under the humid climatic conditions that affected central Chile during the Last Glacial Maximum (LGM). Finally, around 8.5-8 ka, the most recent post-glacial marine transgression (PMT) submerged the site, probably eroding the Late Pleistocene – Early Holocene part of the sequence. Currently, the site lies at ca. 13 m b.s.l. within the shoreface of present-day Quintero Bay, 650 m from the current shoreline. This enhanced understanding of GNLQ1's evolution offers a new perspective on resource availability on the coastal shelf of western South America during the Late Pleistocene, as well as highlighting the unexpected paleontological potential of this area and encouraging future archaeological research of potential prehistoric evidence within these drowned landscapes.

1. Introduction

During the Last Glacial Maximum (LGM), subaerially exposed continental shelves covered vast areas worldwide, available for both human and animal movement. For submerged prehistoric archaeology as an emergent discipline, the reconstruction of the past inundated landscapes and human occupation is crucial not only for a better understanding of early hunter-gatherer groups adapted to the shore and nearshore of the continental shelf, but also for paleolandscape modeling and archaeological sampling (Werz and Flemming, 2001; Bailey et al., 2020; Benjamin et al., 2020; O'Shea, 2021).

Site GNL Quintero 1 (GNLQ1), located in Quintero Bay (32°46′S) on the coast of central Chile, provides the first conclusive evidence to date of a submerged terrestrial Late Pleistocene landscape on the west coast of South America (Cartajena et al., 2013; Carabias et al., 2014; López et al., 2018). Quintero Bay is an active harbor containing marine

* Corresponding author. Departamento de Geología, Facultad de Ciencias Físicas y Matemáticas, Universidad de Chile, Santiago, Chile.
E-mail address: vfloresa@uchile.cl (V. Flores-Aqueveque).

https://doi.org/10.1016/j.quaint.2021.06.005
Received 9 February 2021; Received in revised form 26 May 2021; Accepted 4 June 2021
Available online 11 June 2021

terminal and industrial facilities. GNLQ1 was discovered in 2005 as the result of a systematic archaeological survey of the seabed conducted as part of a Cultural Resource Management (CRM) project for a Liquefied Natural Gas (LNG) terminal. During 2007 preliminary subsurface test excavations were conducted and mechanical coring samples obtained with more extensive excavations, coring and side-scan sonar remote sensing survey following in 2011–2014 field seasons (ÀRKA, 2008; 2014; Carabias et al., 2014).

GNLQ1, now located at 650 m from the current coastline at ca.13 m b.s.l. (below sea level) (Figs. 1 and 2), is characterized by a high abundance and diversity of terrestrial fossils of extinct megafauna and extant fauna immersed in a sedimentary matrix, providing a high-resolution primary context (Cartajena et al., 2013). The site is currently covered only by a centimetric layer of shoreface sand related to low sedimentation rates (Carabias et al., 2020). Bones contained within the deposit include primarily remains of Camelidae, Cervidae, Equidae, Mylodontidae, Xenarthra, Canidae, Myocastorinae, and Octodontidae, among others (López et al., 2018). Some of these taxa were also found in faunal assemblages recovered from terrestrial archaeological sites further north, such as Quereo and Santa Julia (31°50 S), located on the semiarid coast of northern Chile (Cartajena et al., 2013; López et al., 2004; Méndez et al., 2020; Nuñez et al., 1994).

This exceptional finding has contributed significantly to our knowledge of the fauna that inhabited this area, while opening new avenues of inquiry into the study of now-submerged coastal landscapes and their environmental conditions during the lowstand and transgressive stages of the last glacial-interglacial transition within the active margin of the southeastern Pacific coast.

Research focused on Late Pleistocene- Early Holocene submerged sites in North America have highlighted the importance of contextualizing the sedimentary environment in order to understand the depositional histories of site locations. Sedimentological analyses based on sediment cores recovered from the seabed have enabled a more comprehensive picture of the Late Pleistocene continental shelf evolution (Garrison et al., 2016).

Moreover, a detailed description of the sedimentary environment provides an essential framework for the study of inundated archaeological sites (Dunbar, 2012; Halligan et al., 2016; Kendrick, 2006). In this context, site GNLQ1 provides a primary source of data on a drowned landscape viable for both extinct megafauna and early human occupation and movement along the Pacific coast of South America during the Late Pleistocene (Carabias et al., 2014).

In recent years, several studies have been carried out on the faunal assemblage of site GNLQ1, including taxonomic (Cartajena et al., 2013) and taphonomic analyses (López et al., 2012), isotopic characterization (López et al., 2018) and mineralogical determination of bone staining (Cartajena et al., 2021). These studies have provided important information on paleofauna, paleovegetation and post-depositional modifications of the faunal assemblage. However, no exhaustive studies providing a detailed understanding of the sedimentary environment of GNLQ1 have been conducted to date.

Based on general stratigraphic analyses and visual descriptions of a marine core (core T1, Fig. 3) as well as previous studies of paleoecological changes in the study area (Villa-Martinez and Villagran, 1997; Villagrán and Varela, 1990), the depositional environment for the sedimentary strata where the paleontological material is found was previously described either as a shallow estuarine-lagoon or wetland environment in the process of desiccation (Vargas and Ortega, 2008; Carabias et al., 2014), or a low-energy fluvial environment (López et al., 2016) or wetland that developed on a flood plain (Cartajena et al., 2020; Carabias et al., 2020). However, ongoing research and the integration of different proxies led us to postulate a more complex depositional scenario, that of a low-energy fluvial environment or floodplain exposed to brackish transgression and inter-tidal processes that was ultimately covered by the sea (Cartajena et al., 2020; Carabias et al., 2020). More detailed knowledge of the site's sedimentary environment will require the development and integration of new criteria for further paleontological and archaeological exploration of similar coastal areas along western South America.

To gain a better insight of the environmental conditions under which site GNLQ1 formed and the subsequent environmental evolution of the surrounding area, two marine cores collected at the site were analyzed providing key stratigraphic, sedimentological and geochemical data. In addition, a seismic survey of the study area in Quintero Bay was undertaken to determine the geomorphological and stratigraphic context of this shallowly buried submerged landscape.

The results of these analyses provide new insights on the environmental conditions and availability of resources for the development of plant and animal life, paving a path for future archaeological research focusing on finding evidence of early occupations on the present-day

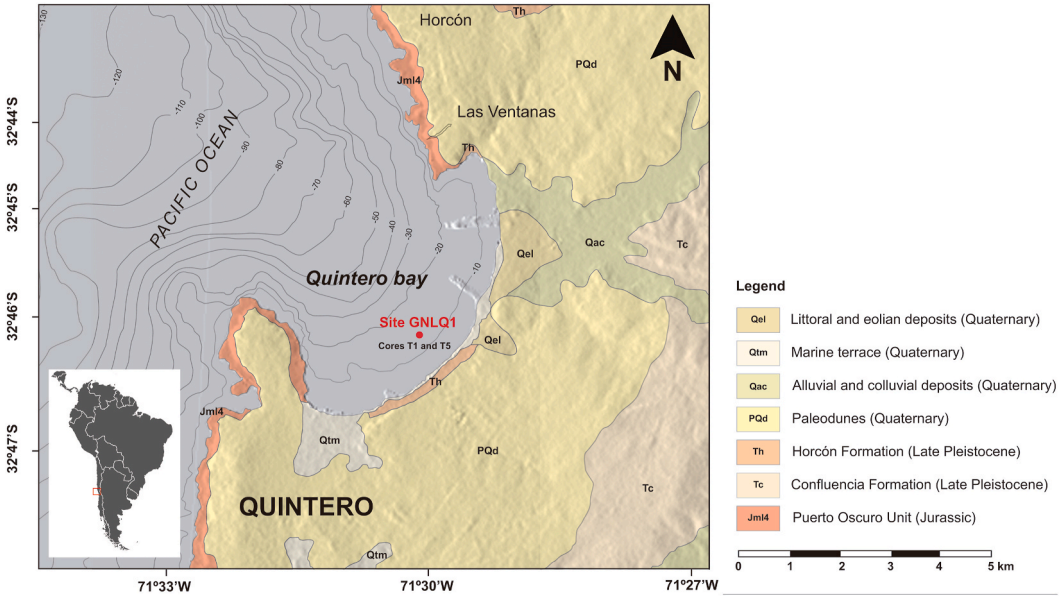

Fig. 1. Geological map of the study area (datum WGS84). The red circle shows the location of site GNLQ1 where cores T1 and T5 were recovered. Modified from Rivano et al. (1993). (For interpretation of the references to colour in this figure legend, the reader is referred to the Web version of this article.)

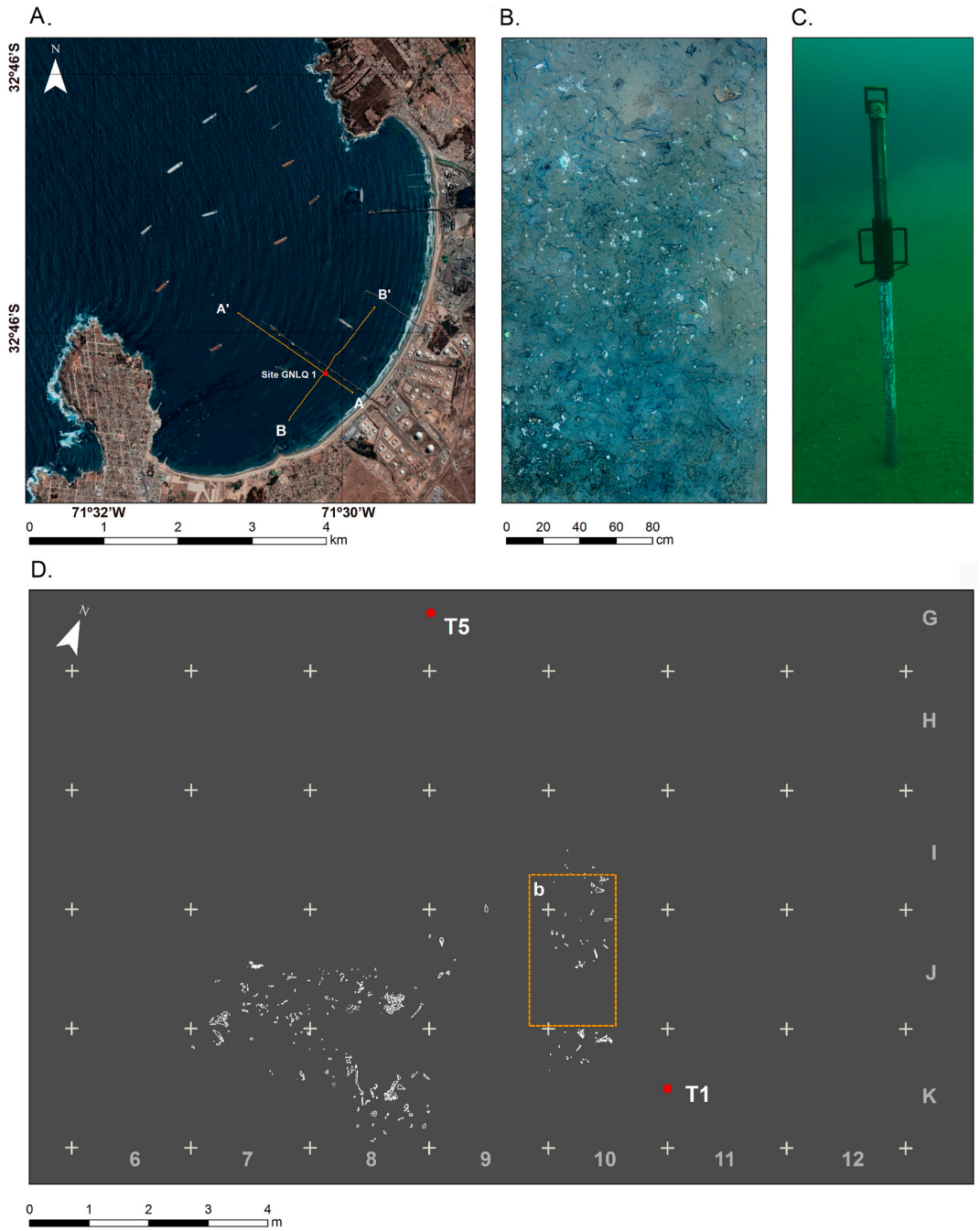

Fig. 2. Site GNLQ1. (a) Location of site GNLQ1 (datum WGS84) and seismic survey tracks (yellow lines AA′ and BB′), (b) Orthomosaic of Quintero bay bottom surface showing in situ bone fragments, (c) Underwater coring in process, (d) Map of bone bed distribution showing relative location of cores T1 and T5 (Photographs b and c by David Letelier, 2016). (For interpretation of the references to colour in this figure legend, the reader is referred to the Web version of this article.)

continental shelf of southwestern South America.

1.1. Regional setting

The tectonic setting of the western coast of South America is characterized by the subduction of the Nazca Plate beneath the South American Plate, which has resulted in the tectonic uplift of coastal areas (Melnick, 2016). Particularly, it has been demonstrated that from central Peru to southern Chile, peninsulas are uplifted at higher rates than the surrounding areas (Saillard et al., 2017), favoring the formation of bays.

For the study area, a mean uplift rate of 0.3 mm/year has been estimated since the Late Pleistocene (e.g., Del Valle et al., 2017, 2018; Martinod et al., 2016). According to this uplift rate and the sea level curve proposed by Lambeck et al. (2014), during the LGM the sea level was approximately 120 m lower than at present (Fig. 1).

Today, Quintero Bay, located in the coast of central Chile (32°S), is a small horseshoe-shaped embayment (~5 km × 2.5 km) open to the northwest (Fig. 1) with depths reaching up to 55–60 m b.s.l. The coastal landscape is relatively smooth, formed by exposed and partially eroded marine platforms that connect with NE-SW-oriented river valleys and hills towards the east.

The area's geology (Fig. 1) primarily features Jurassic intrusive rocks (Jml4, Puerto Oscuro Unit; Rivano et al., 1993) that crop out on the headlands of the bay; the Late Pliocene (Carrillo-Briceño et al., 2013) marine sequence of the Horcón Formation (Th; Thomas, 1958) visible on

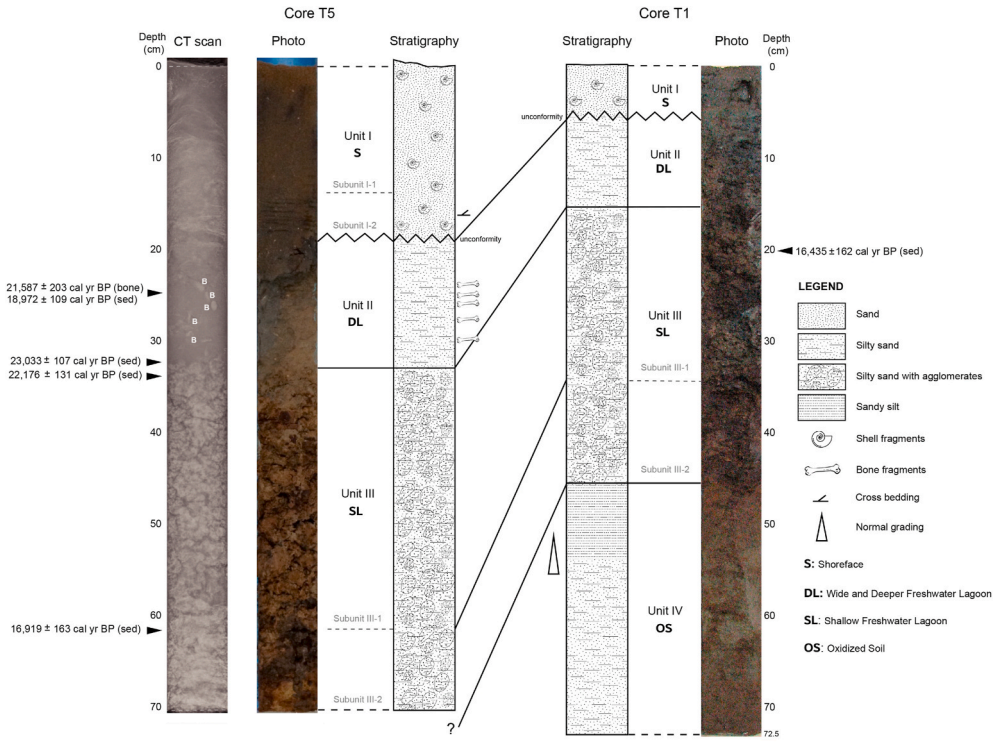

Fig. 3. Stratigraphy of site GNLQ1 showing correlation between cores T5 and T1. Letter 'B' in CT scan of core T5 indicates location of bone fragments. Dates from sediment of core T1 is reported in Cartajena et al. (2013) and Lopez et al. (2016, 2018), while dates from bone and sediments of core T5 are presented in Carabias et al. (2020). For more details, see section 4.1.

the coastal cliffs; and Quaternary eolian (PQd, *'paleodunes'*), alluvial (Qac) and beach (Qel) deposits, widely distributed around the bay (Rivano et al., 1993).

The study area is situated in a semiarid region characterized by dry summers and wet winters, with 281 mm mean annual precipitation (Di Castri and Hajek, 1976). Precipitation is produced by easterly migrating surface cyclones (Garreaud et al., 2008) associated with Southern Westerly Winds (SWW), whose intensity is mainly controlled by the latitudinal position and strength of the South Pacific Subtropical High (SPSH). During austral summer, the SPSH becomes more intense and moves poleward, blocking the SWW belt that shifts to the south. During austral winter, however, a weakened, equatorward-displaced SPSH allows the SWW to reach further north, bringing winter rains to central Chile (e.g., Quintana and Aceituno, 2012). A similar scenario has been inferred for glacial-interglacial timescales. According to Toggweiler (2009), under warm conditions the SWW shift poleward, while in cold climate periods (e.g., the Last Glacial Maximum) the westerlies move equatorward due to magnification of the austral polar cell and increased sea ice around Antarctica (Bentley et al., 2009).

2. Methods

2.1. Coring

In 2007, 2014, two sediment cores (T1 and T5, respectively) were extracted at GNLQ1 from the seabed (Fig. 2a–b) at a depth of ca. 13 m b.s.l. A 7.5-cm diameter, 3-cm long diver-operated piston corer was used for sampling (Fig. 2c). Core T1 has a length of 73 cm, while core T5, extracted ca. 9 m away from T1 (Fig. 2d), is 71.5 cm long (Cartajena et al., 2013; Carabias et al., 2014; López et al., 2016). Once collected, the cores were preserved at 2 °C before being split lengthwise and examined for description and sampling in the laboratory.

2.2. Stratigraphic and sedimentological analyses

In order to study the sedimentary structures and evaluate the presence of fossils, x-ray computed tomography (CT) scans were acquired for core T5 at the Imaging Center of the Clinical Hospital of the Universidad de Chile using a Siemens SOMATOM SENSATION 64. The CT images were acquired at an axial resolution of 0.6 mm, at 120 kV and 320 mA, and were analyzed using the freely available OsiriX DICOM Viewer (11.0.4) software.

Once split and opened, the lithology of cores T1 and T5, including the definition of sedimentary facies, was obtained through visual inspection to determine variations in lithology, grain size, sedimentary structures, and colour (based on Munsell (2009) colour chart), and to identify contact relationships.

T1 and T5 cores were sampled every 1 cm for granulometry and X-Ray Fluorescence (XRF) analysis. During sediment sampling, bone remains found within the core samples were separated for taxonomic analysis.

Grain size analyzes were performed to complement visual descriptions and to characterize variations within each stratigraphic unit. The particle size distribution was determined through laser diffraction spectrometry using a Malvern Mastersizer 2000 instrument provided by the Sedimentology Laboratory in the Geology Department at the Universidad de Chile. For sediment classification and statistical parameters, Folk and Ward (1957) classification was applied.

2.3. Energy dispersive X-Ray Fluorescence (EDXRF)

EDXRF analyses were carried out at 1 cm sampling resolution using an EDX-720 Shimadzu spectrometer at the X-Ray Fluorescence Laboratory in the Department of Geology at the Universidad de Chile. The XRF spectrometer was operated using an Rh X-ray tube set to 15–50 kV and 1000 μA. EDXRF analysis offers a quick, non-destructive, multi elemental method for determining major element composition (from Na

(z = 11) to U (z = 92)).

A total of n = 131 samples were analyzed, 61 belonging to core T1 and 70 from core T5. Due to coring extraction disturbance, the top 12 cm of core T1 was not analyzed. Prior to analysis, each sample was homogenized and grounded with an agate mortar and pestle. Samples were then dry sieved through a 200-mesh sieve to obtain ~0.5 g of sediment sample, which was placed on a stainless-steel sample cup.

In addition to major elements, EDXRF data was used to determine five element ratios to describe differences in carbonate (Ca/Ti and Sr/Ti), redox conditions (Mn/Fe and Mn/Ti) and organic productivity (Si/Ti) (e.g. Brown et al., 2007; Moreno et al., 2007; Kylander et al., 2011; Naeher et al., 2013; Wennrich et al., 2014; Mackenzie et al., 2017).

2.4. Seismic survey

A geophysical survey of the central area of Quintero Bay near GNLQ1 was conducted to characterize the subsurface stratigraphy. Sub-bottom profiler (SBP) data was collected using an Edgetech 3100-P SB424S (4–24 khz) along two perpendicular tracks intersecting at the site location (Fig. 2a). The data was recorded as full-wave and envelope traces and visualized with the freeware SeisSee 2.22.2 using minimum processing, including a trapezoidal bandpass filter [lower cut-off frequency: 500 Hz; upper cut-off frequency: 7000 Hz] and Automatic Gain Control [window length: 3–5 ms]. Penetration allowed the recognition of coherent reflectors up to ~1–2 ms below the seabed (1.5–3 m). Given the difficulty of mapping a shallow bay dominated by sandy surficial sediments which produce multiples reflectors and high attenuation of acoustic energy, special attention was given to the recognition and discarding of artifacts. During processing and interpretation, seismic facies were defined in terms of relative predominance rather than merely reflector geometric array, owing to the difficulty of following low amplitude and/or discontinuous reflectors along the seismic sections.

3. Results

3.1. Stratigraphy and sedimentology

According to stratigraphic and grain size results, four main lithological units can be defined:

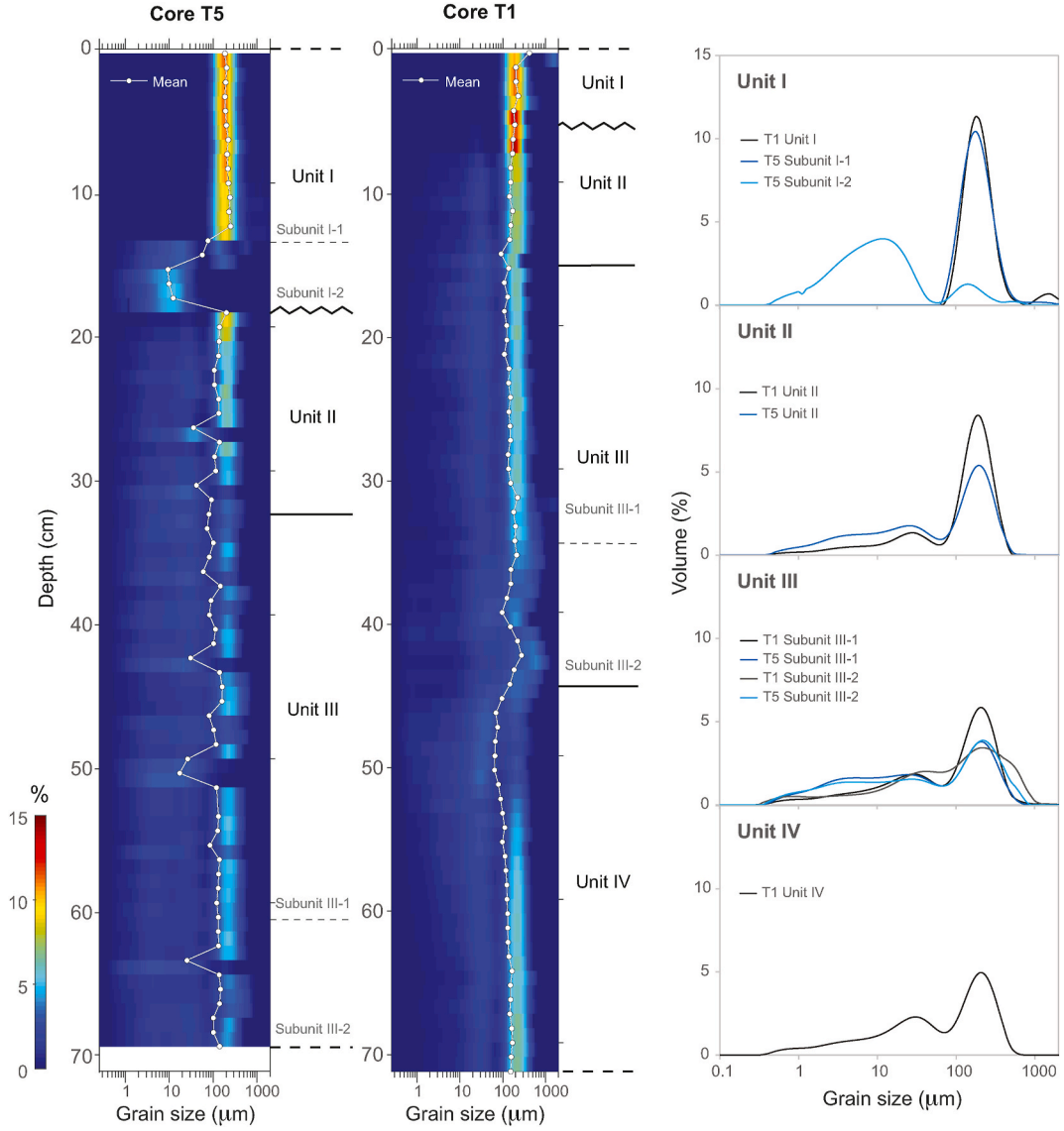

Fig. 4. Grain size distribution of cores T5 and T1. Left panels show a density plot of the grain size volume percentages (colors) and mean grain size values (white line). Right panels display average grain size distributions by stratigraphic units. (For interpretation of the references to colour in this figure legend, the reader is referred to the Web version of this article.)

Unit I: This unit extends from 0 to 5.5 cm depth in core T1 and from 0 to 18.5 cm depth in core T5 and overlies sediments of Unit II unconformably through a sharp erosional contact (Fig. 3). Unit I is composed of brown (7.5 YR 4/2 to 4/4) well sorted fine sand with isolated shell fragments, which are more abundant at the base. Two subunits were defined for this unit: *Subunit I-1* comprises the top part of both cores, specifically at 0–5.5 cm depth in T1 and 0–14 cm depth in T5. *Subunit I-1* is characterized by a unimodal grain size distribution ranging between 178 and 200 μm (Fig. 4). CT images for T5 clearly show cross-bedding structures (Fig. 3). *Subunit I-2* is present only in core T5. Unlike subunit I-1, this subunit presents a bimodal size distribution, with modes ranging between 11 - 22 μm and 141–178 μm (Fig. 4). CT images also enabled identification of cross-bedding structures in this subunit.

Unit II: This unit is composed of light brown (7.5 YR 6/3) to gray (7.5 YR 6/1) silty fine-to-medium sand containing animal bone fragments (Fig. 3). In core T1, this unit spans from 5.5 to 15 cm depth and contains carbon lenses and isolated agglomerates of highly cohesive silty to clayey sand, ranging from 0.5 to 2 cm in diameter. In core T5, Unit II spans from 18.5 to 32.5 cm depth, presenting bone fragments between 23 and 30 cm depth (Fig. 3). Grain size distribution of this unit is bimodal, with main modes between 178 – 224 μm and 22–31 μm (Fig. 4). The contact between Unit II and Unit III is sharp and concordant, although it appears irregular due to the large amount of agglomerates in Unit III.

Unit III: This unit is composed of strong brown (7.5 YR 4/6) to dark brown (7.5 YR 3/4) silty fine-to-medium sand with the presence of medium-to-coarse pebble-size agglomerates consisting of highly cohesive silty to clayey sand. This unit extends from 15 to 44.5 cm depth in core T1, whereas in core T5 it appears between 32.5 cm depth and the base (Fig. 3). Unit III can be subdivided in two subunits. *Subunit III-1* comprises the upper part of Unit III and is found between 15 and 34 cm depth in T1 and between 32.5 and 62 cm depth in core T5. This subunit is characterized by agglomerates supported by approximately 20–30% of matrix. The matrix presents a bimodal distribution, with the main mode ranging between 200 and 251 μm, while the secondary mode ranges between 28 and 32 μm in core T1, and between 2 and 35 μm in core T5 (Fig. 4). *Subunit III-2* is identified between 34 and 44.5 cm depth in T1 and from 62 cm depth to the base in T5 (Fig. 3). *Subunit III-2* corresponds to agglomerates with only ~4% of matrix characterized by a trimodal size distribution, with the main mode ranging between 200 and 632 μm, and a massive appearance. The secondary and tertiary modes range between 31 – 39 μm and 0.7–0.8 μm, respectively (Fig. 4), with the third mode more evident in T5. Unit III overlies Unit IV unconformably with an irregular erosional contact (Fig. 3).

Unit IV: This stratigraphic unit is present only in core T1, from 44.5 cm depth to the bottom of the core (Fig. 3). It is composed of strong brown (7.5 YR 5/6), massive silty fine-to-medium sands, fining upward from silty sand at the bottom to sandy silt at the top. Unit IV has a trimodal grain size distribution with the main mode ranging between 178 and 251 μm. The secondary mode ranges from 31 to 35 μm, and the third is a fine mode that ranges between 0.7 and 0.8 μm (Fig. 4). The base of Unit IV is unknown.

3.2. Inorganic chemistry

EDXRF results indicate that both cores are characterized by a relatively high content of silicon (Si), iron (Fe), aluminum (Al), titanium (Ti), calcium (Ca), and potassium (K). Other elements (e.g. manganese (Mn), phosphorous (P), zirconium (Zr) and sulfur (S), among others) are also present but less frequent.

As shown in Fig. 5, core T5 is characterized by Al, K, strontium (Sr), and Si following roughly a similar pattern, characterized by high values for Unit II and the bottom of Unit I, steadily decreasing towards the top of the core, while Unit II has nearly constant values throughout. Fe values mirror the previous pattern, while Ca and Ti display high values in Unit I and relatively low and constant values in units II and III. On the other hand, Mn abundance for units I and II is low but increases steadily in Unit III, reaching high values near the bottom. Phosphorous is present near the top and towards the base of the core. Sulfur as well as heavy metals such as copper (Cu), vanadium (V), zinc (Zn), Zr, yttrium (Y), and chromium (Cr) are present almost exclusively in the upper part of the core.

In core T1 (Fig. 5), Al, K, Ca, Ti and Si are characterized by low signals in the middle part of the core and higher values towards both ends, while Mn, Fe and P display the opposite, exhibiting high values at the middle of the core and decreasing towards the ends. Sr shows high variability, especially towards the upper part of the core.

It should be noted that the null signal of Ti in the middle part of T1 (~40–49 cm depth) could be explained by the presence of Ti concentrations below the detection limit of the EDX-720 spectrometer (20–50 ppm) and/or because the Ti signal is 'hidden' behind the peak of more abundant elements with a band energy close to Ti, such as Fe.

Based on the relative changes (signal, variability, and trend) in each element, three main units can be defined for core T5 (Fig. 5). The main characteristics of each of these geochemical units are summarized in Table 1.

Element ratios also confirm the defined geochemical units (Fig. 6). Core T5 is characterized by low Si/Ti, Ca/Ti, and Sr/Ti ratios towards

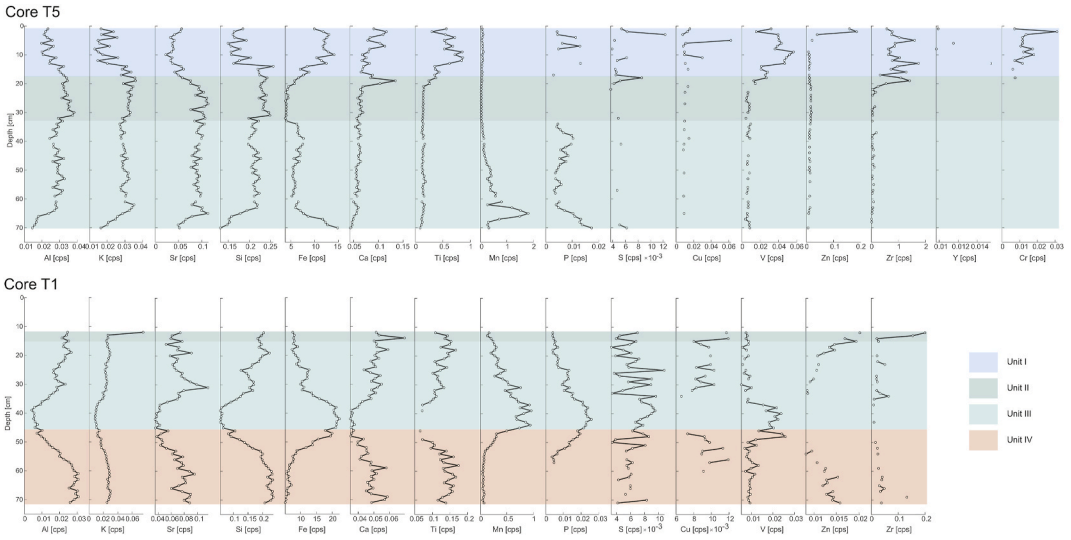

Fig. 5. Major elements present in cores T5 and T1 determined by XRF analysis. Measurements are expressed in count per second (cps).

Table 1
Main geochemical characteristics of core T5.

Unit	Depth (cm)	Main geochemical features
I	0–18.5	Low and variable signals of Al, K, Sr, Si and Ca High and variable signals of Fe, Ti and P High and very variable signals of Cr, Cu, S, V, Y, Zn and Zr
II	18.5–32.5	High content of Al, K, Sr and Si Low and almost constant signals of Fe, Ca, and Ti
III	32.5–70.0	Relatively high content of Al, K, Sr, Si, and Fe Low and almost constant signals of Ca and Ti Peak of Sr and Mn between 62 and 67 cm depth High and variable amounts of P

Table 2
Main geochemical characteristics of core T1.

Unit	Depth (cm)	Main geochemical features
II	12.0–15.0	High and downward decreasing signals of K, Sr, and Si Low and downward increasing signals of Fe, Ti, Mn, and P
III	15.0–45.5	High and downward decreasing signals of Al, K, Si, Ca, and Ti Low and downward increasing signals of Fe, Mn and P Relatively high and variable signal of Sr
IV	45.5–73	Low and downward increasing signals of Al, K, Sr, Si, Ca and Ti Relatively high and downward decreasing signal of Fe Low signal of Mn and P

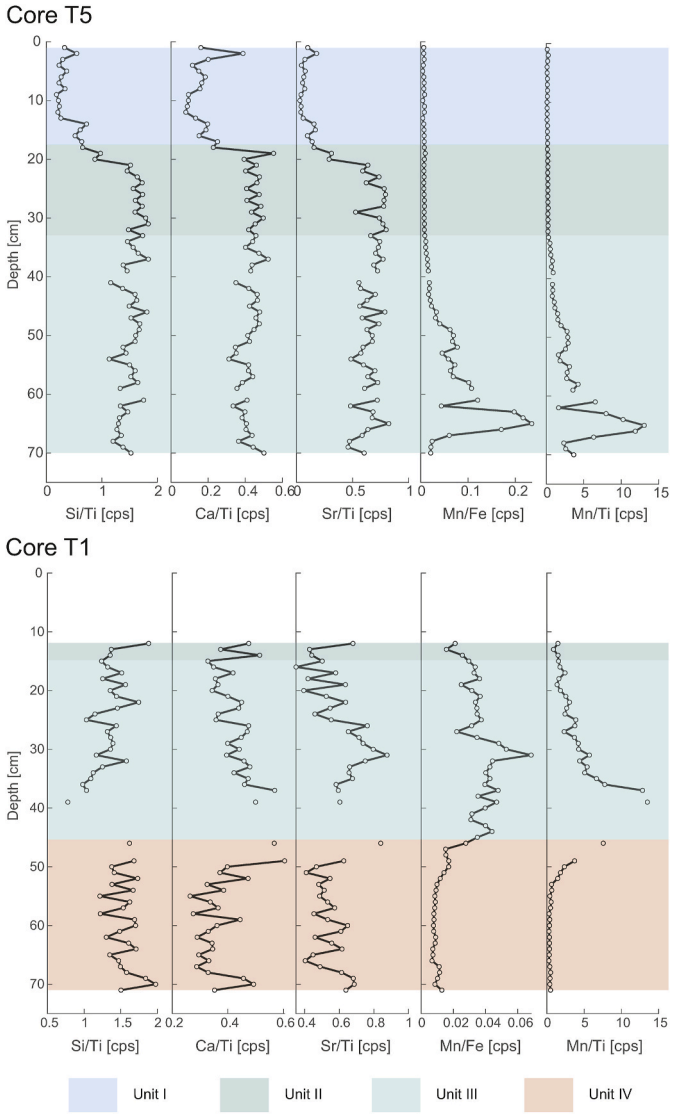

Fig. 6. Elemental ratios in cores T5 and T1 showing organic productivity (Si/Ti), carbonate precipitation (Ca/Ti, Sr/Ti) and paleoredox (Mn/Fe, Mn/Ti) indicators.

the top (0–18,5 cm depth) and higher values for the rest of the core (18.5–70 cm depth). Mn/Fe and Mn/Ti ratios are generally low for the upper half of the core but show a marked increase with depth in the bottom half, with a remarkable peak related to the sudden increase of Mn around 65 cm depth.

Core T1 can be divided into three major geochemical units (Fig. 5), as presented in Table 2. The lower half of core T1 has low Mn/Fe and Mn/Ti ratios, relatively low and variable Ca/Ti and Sr/Ti ratios (Fig. 6). Mn/Fe, Mn/Ti and Sr/Ti ratios are relatively higher in the upper half, but decrease towards the top, while the Si/Ti ratio is relatively higher and increases towards the top (Fig. 6).

3.3. Seismic stratigraphy

Fig. 7 shows the results of the geophysical survey. Seismic profile A-A′ is 1770 m long and lies perpendicular to the coast, while seismic profile B–B' is 1230 m long and runs roughly parallel to the coast. Four seismic facies were defined based on the predominant geometries resulting from the mapping of coherent or semi continuous reflectors. The mapped reflectors are usually discontinuous and of variable amplitude, and are accompanied by non-coherent discontinuous reflectors and chaotic facies. Type I facies consist of areas characterized by the presence of high and low amplitude subhorizontal reflectors. Type II facies consist of areas characterized by dipping reflectors, either straight or curved. Type III facies consist of areas where subhorizontal and dipping reflectors can be easily recognized, although no clear spatial connection can be discerned between them. Type IV facies describe areas where no coherent geometries were discernible, although coherent reflectors could be recognized locally. In all cases, the low coherence of the mapped reflectors prevents the following of a single reflector for more than a few tens of consecutives traces (e.g. a few meters).

In section A-A' (Fig. 7), facies II and III dominate the central part, while facies IV are more predominant near the beginning and end of the section. The geometries observed within the first 70–80 cm below the seafloor are discontinuous and display low coherence. However, occasionally high angle dipping reflectors reach the seafloor, while curved dipping reflectors are relatively common within the first few meters below the seafloor. Near the location of GNLQ1 (A.1; Fig. 7), the top 1 ms (~1.5 m) is characterized by subhorizontal reflectors limiting high angle reflectors. In other parts of the A-A' section, dipping reflectors are discontinuous but easily identifiable, and suggest the presence of downlapping and truncation geometries (A.2; Fig. 7).

In section B–B' (Fig. 7), Type II facies dominate the area near GNLQ1, although there are parts of the section in the vicinity of the site where no laterally coherent reflectors could be mapped. Type II facies are more common in the SW part of the section, while the NE part is dominated by chaotic reflectors (Type IV facies). In one part of the section at least, a strong seafloor reflector (ssfr; Fig. 7) is able to reflect most of the acoustic energy, causing a loss in penetration and in apparent reflector coherence below it. In the NE part of the section, high angle dipping reflectors near the seafloor (shar; Fig. 7) represent the only coherent reflectors that can be mapped. In the section near GNLQ1 (B.1; Fig. 7) there are curved, low-angle dipping reflectors that form a geometry resembling downlapping, while at the location of the site, NE dipping reflectors are clearly identifiable.

4. Discussion

4.1. Site GNLQ1 depositional history

The depositional history of GNLQ1 can be tentatively reconstructed

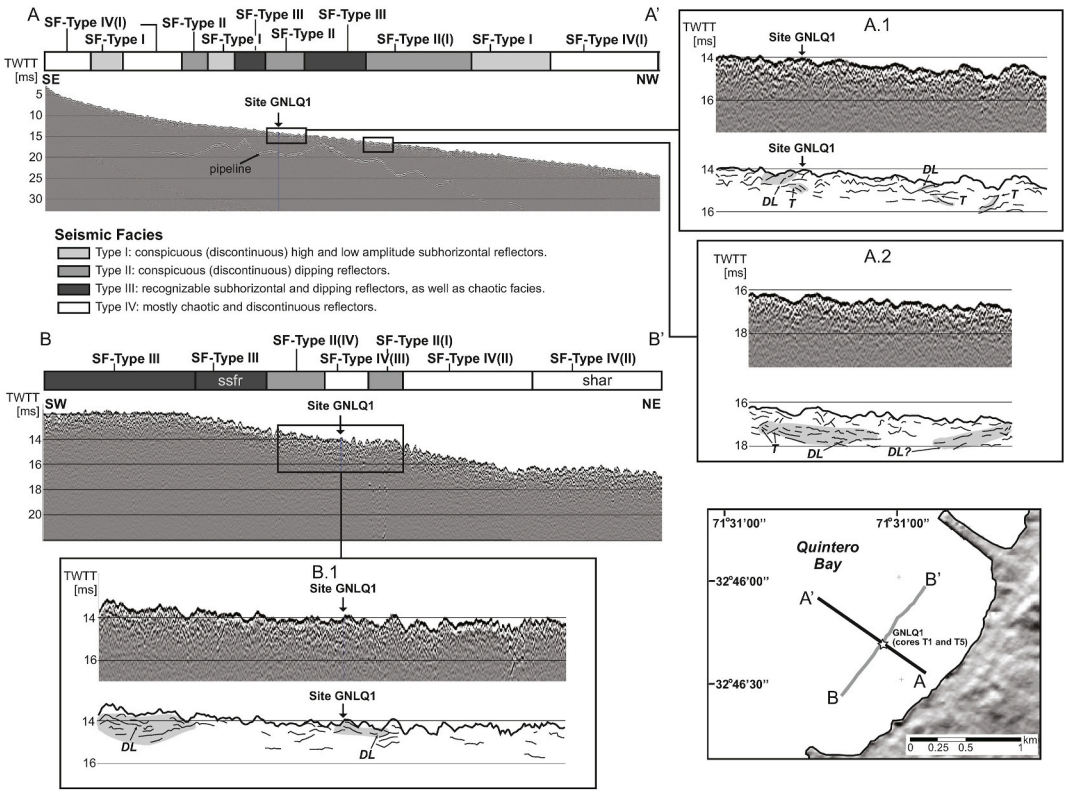

Fig. 7. Sub-bottom profiler sections. Section A-A′ is perpendicular and B–B′ is roughly parallel to the coastline, while both intersect at the location of GNLQ1. Sections are shown with band pass filtering (lower cutoff frequency: 500 Hz, upper cutoff frequency: 7000 Hz) exclusively. The vertical axis is two-way travel time (TWTT) milliseconds. The mapping of reflectors was mostly conducted within 2 ms from the seafloor (black thick line in A.1, A.2 and B.1). The main characteristics of the defined seismic facies are indicated. DL: downlapping; T: truncation; ssfr: seafloor strong reflector; shar: superficial high angle reflector.

by integrating the stratigraphic, sedimentary, and geochemical data. While stratigraphy and sedimentology allow the reconstruction of the general depositional environment, geochemistry provides valuable insight into intra-environmental changes that occurred at relatively shorter timescales.

According to the available radiocarbon chronology for GNLQ1 (Table 3; Carabias et al., 2020), the age of the site spans the Late Pleistocene to the present day. Bones of different taxa, collected from the cores as well as at the bottom surface (attributable to Unit II) near the cores, were dated between ca. 29,200 and 21,300 cal yr BP by using the bioapatite fraction. OxCal 4.4, with the ShCal20 terrestrial calibration curve for the Southern Hemisphere (Hogg et al., 2020), was used to calibrate bone and sediment samples. Although radiocarbon dating of biological apatite has been widely applied in collagen-devoid samples (Cherkinsky, 2009), bioapatite diagenesis may affect radiocarbon ages and contamination by older carbonates as observed by Chatters et al. (2017) in submerged bones. However, recently Méndez et al. (2020) compared bioapatite and collagen dates for megafauna, showing no significant differences despite the fact that bioapatite offset is expected due to relatively older ages. Bulk organic sediment samples depict a younger and narrower range, between ca. 23,100 and 16,200 cal yr BP. According to Carabias et al. (2020), these ages could be explained by the incorporation of younger organic matter into older sediments by biological activity and/or percolation.

The environmental variations recorded can be described in four phases, from older to younger (Fig. 8):

Table 3
Radiocarbon AMS dates on sediments and bioapatite fraction of bones and molars.

#Lab Code	Sample	Depth (cm)	Sample provenance	^{14}C Age years BP	cal. yr BP (95% Prob.)	References
UGAMS 9194	Sediment	20	T1- Unit III	13,640 ± 40	16,435 ± 162	Cartajena et al. (2013)
UGAMS 15535	Bone	Surface	Near T1- Unit II	24,890 ± 70	29,052 ± 164	López et al. (2016)
UGAMS 15536	Bone	Surface	Near T1- Unit II	23,720 ± 70	27,805 ± 111	López et al. (2016)
UGAMS 15537	Bone	Surface	Near T1- Unit II	21,580 ± 60	25,862 ± 106	López et al. (2016)
UGAMS 15538	Bone	Surface	Near T1- Unit II	23,060 ± 60	27,296 ± 101	López et al. (2016)
UGAMS 15539	Bone	Surface	Near T1- Unit II	21,690 ± 50	25,923 ± 88	López et al. (2016)
UGAMS 20838	Bone	Surface	Near T1- Unit II	24,010 ± 60	29,061 ± 155	López et al. (2018)
UGAMS 20839	Bone	Surface	Near T1- Unit II	23,110 ± 50	27,387 ± 166	López et al. (2018)
UGAMS 20844	Bone	Surface	Near T1- Unit II	19,280 ± 40	23,315 ± 341	López et al. (2018)
UGAMS 20841	Bone	Surface	Near T1- Unit II	20,040 ± 45	24,020 ± 170	López et al. (2018)
UGAMS 29495	Bone	24	T5- Unit II	17,800 ± 40	21,587 ± 203	Carabias et al. (2020)
UGAMS 29496	Sediment	24	T5 - Unit II	15,740 ± 40	18,972 ± 109	Carabias et al. (2020)
UGAMS 29497	Sediment	32	T5 - Unit II	19,160 ± 50	23,033 ± 107	Carabias et al. (2020)
UGAMS 29498	Sediment	34	T5 - Unit III	18,250 ± 45	22,176 ± 131	Carabias et al. (2020)
UGAMS 29499	Sediment	62	T5 - Unit III	13,980 ± 40	16,919 ± 163	Carabias et al. (2020)

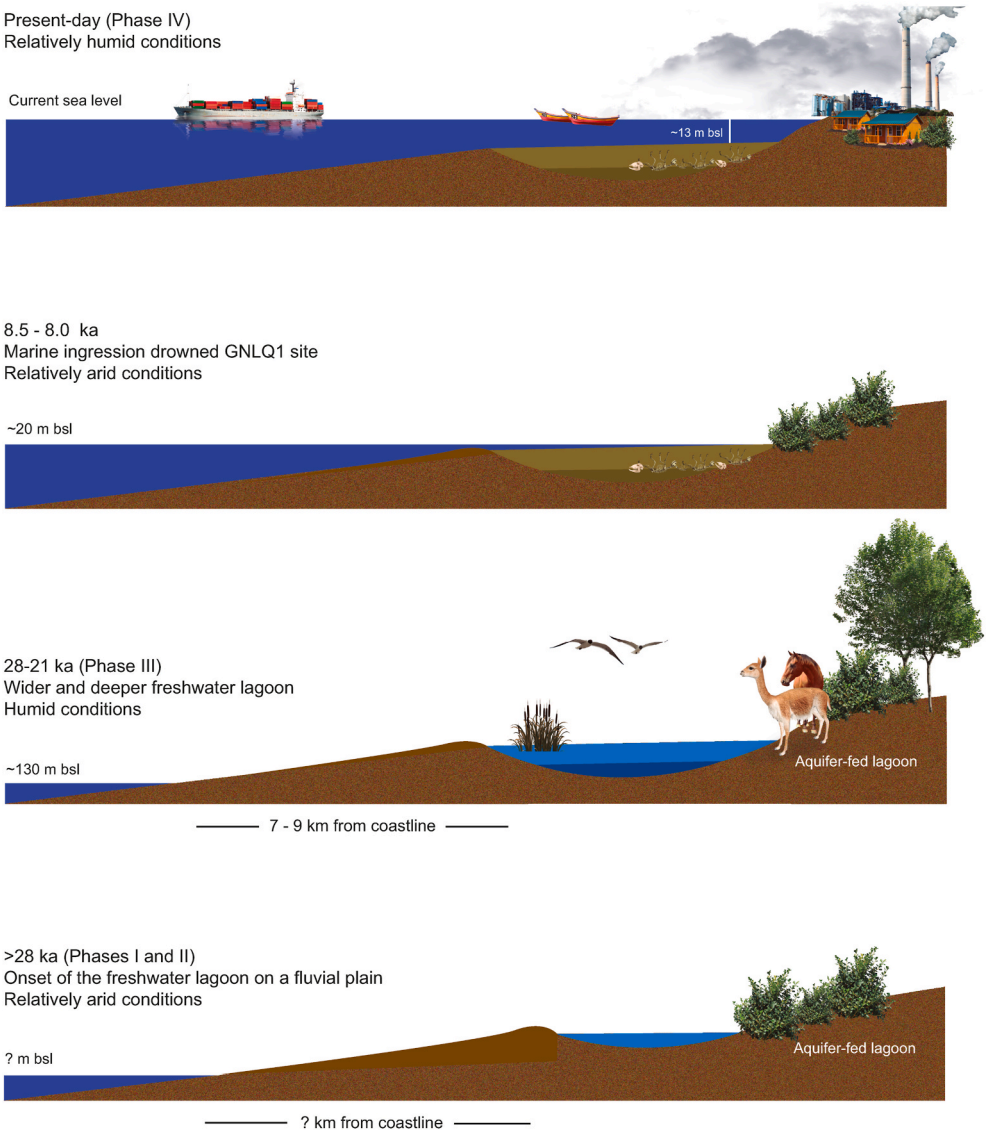

Fig. 8. Evolution model of site GNLQ1. Sea level shown is relative to present-day sea level.

4.1.1. Phase I: Subaerial conditions in a fluvial plain

The basal unit, present only in T1 (Unit IV), is interpreted as the result of subaerial conditions, particularly exposed oxidized soil upon which a low-energy freshwater environment developed. This is evidenced by fine sediments presenting upward fining (Fig. 3), which is characteristic of fine-grained sediment point bars (Colombera and Mountney, 2019). In addition, the upward decreasing signals of Si, Al, K, Ca and Ti exhibit a strong correlation with fine and medium sand content, thus suggesting a lithogenic origin. Mineral analyses performed on the sediments of Quintero Bay indicate a predominance of silicates and aluminosilicates such as Albite, Anorthite, Bytownite, and Quartz, among others (Parra et al., 2015), thereby supporting this interpretation.

The pattern of low but increasing upward intensities of Mn and low Mn/Fe ratios (Figs. 5 and 6), suggests a transition from anoxic to slightly oxic conditions (Naeher et al., 2013) towards the top of the unit. High Fe values, coinciding with higher Mn signals, observed towards the top indicate the occurrence of iron oxides that accumulate at the top of this bed. In fact, the strong brown color (7.5 YR 4/6) described for this unit was previously interpreted as having been produced by the transition from subaerial to subaquatic conditions (Carabias et al., 2014; Cartajena et al., 2013).

According to seismic data, Unit IV corresponds to seismic facies characterized by curved and dipping reflectors as well as downlapping resembling geometries. These seismic facies are observed in several parts of both seismic sections occurring within 1 ms below the seafloor (~1.5 m; Fig. 7), and are suggestive of lateral accretion within channel fill deposits (Gibling, 2006), although the accumulation of draping sediments on small curved depressions cannot be completely ruled out. However, based on the distribution of seismic facies and their location within the bay, lateral accretion could be the dominant geological process governing the formation of the curved and dipping geometries. This would indicate a paleoenvironment dominated by small meandering streams (Gibling, 2006), which would explain the limited lateral continuity of the corresponding seismic facies, and the isolated nature of other facies such as Type I (subhorizontal reflectors, Fig. 7). The extent of the available seismic coverage indicates that this type of environment extended for at least a kilometer around the site. Since the site is now submerged, this indicates that the low energy fluvial environment developed before the transgression, when the area must have been part of a distal fluvial system.

4.1.2. Phase II: Onset of a low-energy freshwater environment (freshwater lagoon)

These conditions are represented by Unit III, observed in both cores (Fig. 3). The interpretation of a freshwater lagoon environment is supported by the fine grain size of the sediments of this unit and the relatively low signals of terrigenous components (Si, Al, K, Ca, and Ti) (Fig. 5). The lack of coarser sediments and the moderate sorting of this deposit (Fig. 4) indicates limited runoff input, suggesting that the lagoon was mostly fed by groundwater. A freshwater lagoon environment is also suggested by the high Ca/Ti and Sr/Ti ratios (Fig. 6) indicating the precipitation of authigenic carbonates (Fig. 6) accompanied by low detrital input (Kylander et al., 2011; Mackenzie et al., 2017).

The relatively high Si/Ti ratio (Fig. 6) suggests the presence of biogenic silica, probably associated with diatom productivity (Brown et al., 2007; Wennrich et al., 2014), which could be responsible for diluting the detrital content, thus reducing the concentrations of elements associated with terrigenous sediments. Another biogenic component contributing to low terrigenous content is indicated by the high concentrations of P observed towards the bottom of this unit (Fig. 5), which could be related to vegetation assimilation and storage of this element in a freshwater ecosystem (Reddy et al., 1999).

The relatively high and variable Mn content and Mn/Fe ratios observed in both cores (Figs. 5 and 6) suggest the presence of manganese oxides, since manganese precipitates under aerobic conditions (Davison, 1993). This interpretation is consistent with recent mineralogical analyses of the sediments of this unit (Cartajena et al., 2021), which show the presence of Fe and Mn oxides such as hematite (Fe_2O_3), pyrolusite (MnO_2), and goethite (FeO(OH)). Higher oxygen content in the water column could be related either to photosynthetic processes or intense bottom water ventilation (Moreno et al., 2007) and could indicate shallow waters (Mackenzie et al., 2017). However, Cartajena et al. (2021) also found iron sulfides such as pyrite (FeS_2) and greigite (Fe_3S_4), which suggest that reduction processes have also affected this unit.

Consequently, the variability in Mn content could be interpreted as changes in the lagoon water level, which resulted in regular oxic to anoxic shifts in bottom water conditions. This changing water level could explain the pebble-size agglomerates observed in this unit (Fig. 3), which can be interpreted as intraclasts caused by changes in extensiveness and the consequent intermittent exposure and drying out of its margin, allowing the formation of sediment clasts as new material filled mud cracks before they were again flooded. Accordingly, observed agglomerates were probably formed by the progressive fragmentation of the cracked surface layer during shallow water periods that was later incorporated into wetland-forming sediment layers (Semeniuk and Semeniuk, 2004).

4.1.3. Phase III: Deeper, larger freshwater lagoon

This environment is interpreted from Unit II, present in both cores (Fig. 3). As in the previous phase, fine-grained sediments support the interpretation of a low-energy deposition.

Very low signals of Mn and low Mn/Fe ratios (Figs. 5 and 6) indicate anoxic conditions that can be interpreted as produced by limited circulation in the water column and/or low ventilation of bottom waters (Moreno et al., 2007), both being consistent with a deeper lagoon. Anoxic conditions for this unit were also interpreted by López et al. (2012) based on the presence of framboidal pyrite in the osseous matrix of a cf. *Palaeolama* sp. humerus found in this unit. In addition, mineralogical analyses of stained bones found in this unit suggest the presence of sulfides as well as oxides, the latter being associated with aerobic conditions occurring during and after site exposure (Cartajena et al., 2021).

Wetter conditions consistent with a more permanent wetland environment are indicated by low Mn/Ti ratios (Fig. 6) as well as the lack of intraclasts in this unit (Fig. 3), which suggests a relatively greater distance to the margin of the lagoon.

As in the previous unit (Unit III), the higher Si/Ti ratio (Fig. 6) suggests the presence of biogenic silica (e.g. Brown et al., 2007), possibly related to diatoms. Additionally, according to Kylander et al. (2011), high Ca/Ti and Sr/Ti ratios (Fig. 6) reflect carbonate precipitation.

The absence of P in this unit (Fig. 5) could be attributed to several processes. For example, Quinton et al. (2001) explains the lack of P in soils in terms of a period of small erosive events during sedimentation. Phosphorous losses from soils have also been associated with intense weathering and leaching (Syers and Walker, 1969), which, in the case of site GNLQ1, could have occurred after site exposure. On the other hand, Reddy et al. (1999) explain the low P content in wetlands as a product of its removal from soil by the roots of some macrophytes, such as Typha. In fact, the presence of root marks in most (86%) of the osseous fragments in this site indicate an environment with abundant vegetation (López et al., 2016), which could support the absence of phosphorous due to sequestration by plants.

During this more humid stage, a diverse array of animals attracted by the freshwater and the vegetation congregated at this wider, deeper lagoon. Animals that died along the lagoon margins were rapidly covered by sediment that was exposed to subaerial conditions only for a short period of time, hereby enhancing bone preservation. This is attested to by the low degree of weathering observed in bones (López et al., 2016).

The presence of a well-preserved high-taxonomic faunal bone assemblage of terrestrial fauna (Carabias et al., 2014; Cartajena et al., 2013, 2021; López et al., 2016) with no evidence of significant hydraulic transport (López et al., 2016) suggests site formation processes comparable in part to those proposed by Brumfitt et al. (2013) for the Mio-Pliocene Langebaanweg bone assemblage on West Coast of South Africa, in which a high number of animal carcasses accumulated in and around a low-energy waterhole.

The freshwater lagoon environment and, therefore, the relatively wetter conditions in the study region prevailed from 28 to 21 ka cal BP approximately, according to the ages reported for the bone assemblage (Carabias et al., 2020). The accumulation of bones during this period, together with their high degree of preservation, account for this dense bonebed deposit.

The humid conditions inferred for the formation of GNLQ1 are consistent with the period of maximum humidity reported in north-central Chile for the last glacial period (~33-19 ka) by Kaiser et al. (2008), based on marine records from north-central Chile (30°S). According to these authors, this period, which followed arid conditions (40–33 ka), was also characterized by abundant humid-adapted C3-type vegetation, high sediment input into the ocean, and low sea surface temperatures. Wetter conditions were also interpreted by Veit et al. (2015) based on soil horizon development dated at 22 ± 1 ka in Las Ventanas, north of Quintero Bay. According to Kaiser et al. (2008), these wetter conditions ended at around 17–16 ka BP, as the result of the decreased influence of the SWW at lower latitudes produced by a southward displacement of the SPSH.

4.1.4. Phase IV: Shoreface of present-day Quintero Bay

This phase is represented by Unit I, which is observed in both cores, although it is better developed in core T5 (Figs. 3 and 4). It is characterized by relatively coarse (fine-to-medium sand) and well-sorted sediments with shell fragments that indicate a relatively shallow marine environment. Geochemistry data support this interpretation. The high signal of Ti (Fig. 5), a relatively immobile element, is linked to higher terrigenous input (Wennrich et al., 2014), and therefore to closer proximity to the shoreline.

In addition, a relatively high Fe signal (Fig. 5) could indicate detrital input, but also changes in the source of sediments or redox conditions (Kylander et al., 2011). The strong relationship between Fe and Ti (Fig. 5) and the lack of finer particles in this unit highlight the allochthonous origin of this element.

Unit I also presents a low Si signal and the lowest Si/Ti ratio of the

entire sequence (Figs. 5 and 6), indicating that Si could be mainly related to terrestrial particles. The predominance of sand-sized particles in this unit (Fig. 4) suggests a detrital origin for silicon.

Low Ca/Ti and Sr/Ti ratios (Fig. 6) indicate a relative decrease in carbonate precipitation (Mackenzie et al., 2017), probably related to the change in coastal marine environmental conditions coupled with an increase in water depth. In turn, very low Fe/Ti, Mn/Ti and Mn/Fe ratios (Fig. 6) reflect the current anoxic conditions below the water/sediment interface (Kristensen, 2000), related to low ventilation at the bottom of the bay in the shoreface area.

The unconformity between the previous unit (Unit II) and the shallow marine conditions interpreted from Unit I represents the record of the last marine transgression in the area, which affected GNLQ1 at around 8.5–8.0 ka BP (Carabias et al., 2020) during the Early Holocene Sea Level Rise period (Smith et al., 2011), the last interval of rapid sea level rise during the PMT. This transgression probably eroded most of the upper part of the sequence deposited between the Late Pleistocene (21 ka cal BP) and the Early Holocene (8.5–8.0 ka BP), when shallow marine conditions were established for site GNLQ1. However, it should be noted that stratigraphy also suggests current erosion by coastal dynamics, in which a thicker layer of sand (Unit I) could be protecting the underlaying bed (Unit II) from waves tidal and swell erosion, thus aiding the preservation of the record.

4.2. Mid-Holocene to present day conditions

Paleoecological records obtained from the present-day coastal plain of Quintero indicate that from ca. 6.2–5.0 ka cal BP, the surroundings of Quintero Bay transitioned from a marine and brackish environment to a freshwater marsh environment (Dura et al., 2015). During this period, the sea level was higher than today (e.g. Isla, 1989) and climatic conditions were warmer and dryer than at present (Villa-Martinez and Villagran, 1997). Between 5 and 4 ka BP, a shallow lagoon developed in the area, which after 4 ka BP transitioned to a marsh that remained until 2 ka BP, the product of increasingly wet conditions that characterized this period. From 2 ka BP onward, colder and wetter climatic conditions, similar to the present, were established (Villa-Martinez and Villagran, 1997).

More recently, since the beginning of 20th century, the landscape of Quintero has been strongly influenced by human activities. Historical maps indicate that between the mid-19th and early-20th century, the landscape around Quintero Bay was dominated by two major lagoons, the larger of them (Laguna de Campiche) covering an area of ~4.5 km^2 during this period. Current wetland areas are minimal in Quintero Bay (<5% of the available surface) as a result of industrial activities conducted in the area since the mid-20th century (Carabias et al., 2020).

Human activities are also evidenced by major signatures of heavy metals observed exclusively in the upper part of core T5 (Unit I; Fig. 5) which highlight the anthropogenic influence of Quintero's recent industrial history. In the mid-20th century, the Ventanas industrial park was developed near the northern part of Quintero Bay. This park, comprising a copper smelter and a thermoelectric power plant among other installations, is the source of several contaminants to the atmosphere and the marine environment (e.g. Ginocchio et al., 2004; Parra et al., 2014, 2015). In this sense, Cr and V could be related to the coal power plant (Parra et al., 2015) while Cu and Zn have been directly related to copper smelting activities (Parra et al., 2014, 2015). Sulfur has also been widely linked to smelting activities in the zone (González et al., 2014; Olivares et al., 2002), as well as to coal-fired power plants (Parra et al., 2014). Zr is a well-known by-product of mining (Hedrick, 2000). Phosphorous concentrations could be associated with the mineral composition of the sediments of Quintero Bay, which include phosphate (Parra et al., 2015), or to its general use as a fertilizer (Wuana and Okieimen, 2011). Finally, yttrium has been associated with carbon emissions (Vargas et al., 2007). It should be noted that in certain concentrations most of these elements have been considered toxic for the ecosystem and the health of the nearby population (e.g., González and Ite, 1992; Ginocchio et al., 2004).

Lastly, the stability of the sedimentary matrix where the bones are embedded, is jeopardized today by being partially exposed to hydrodynamic actions attributable to the modification of the depositional environment. Further studies should consider the effects of detected pollution and the impact on the sedimentary matrix of human actions on the environment.

5. Summary and conclusions

Sedimentological and geochemical analyses performed on two sediment cores provided a complete stratigraphic sequence for the GNLQ1 Late Pleistocene submerged site. Seismic data, in turn, allowed a better understanding of the morphostratigraphic setting in which this shallowly buried submerged landscape was formed.

The results obtained indicate that GNLQ1 formed during the Late Pleistocene in a freshwater lagoon environment developed on an exposed fluvial plain. According to Carabias et al. (2020), by this time the shoreline was at 7–9 km off the present-day coastline. In the beginning, the lagoon was shallow and relatively small, existing under relatively arid conditions. During a second, more humid stage that occurred between 28 and 21 ka cal BP, at least, a wider, deeper lagoon sheltered a high diversity of fauna attracted by the freshwater and vegetation. This environment is consistent with the humid climatic conditions proposed for this period in central Chile. Subsequently, at around 8.5–8.0 ka BP (Carabias et al., 2020), site GNLQ1 was drowned during the sea level rise that followed the LGM, likely resulting in the erosion of most of the upper part of the sequence deposited during the Late Pleistocene - Early Holocene transition.

Currently, GNLQ1 is situated at ca. 13 m b.s.l., in the shoreface area of present-day Quintero Bay. The human activities carried out in the zone have strongly impacted the landscape and inhibited lagoon development, with current wetlands restricted to less than 5% of their recorded historical surface.

Sedimentological and geochemical data have provided key information on GNLQ1's depositional environment and its formation and evolution and contribute to a better understanding of this unique submerged landscape located on the nearshore Pacific continental shelf of South America. This evidence is in good agreement with seismic data and suggests that by the LGM, freshwater lagoon systems in coastal Central Chile represented an attractive habitat for a high diversity of fauna and was available for human occupation.

Data availability

The data that support the findings of this study are available on request from the corresponding author. The data are not publicly available due to the fact that part of them will be used in other publication.

Author contributions

Valentina Flores-Aqueveque: Conceptualization, Methodology, Investigation, Writing - Original Draft preparation. **Cristina Ortega:** Methodology, Formal analysis, Writing - Review & Editing. **Rodrigo Fernández:** Methodology, Formal analysis, Writing - Review & Editing. **Diego Carabias:** Writing - Review & Editing, Project administration. **Renato Simonetti:** Methodology, Formal analysis. **Isabel Cartajena:** Conceptualization, Writing - Review & Editing, Funding acquisition, Project administration. **Laura Díaz:** Methodology, Formal analysis, **Charles González:** Formal analysis, Visualization.

Declaration of competing interest

The authors declare that they have no known competing financial

interests or personal relationships that could have appeared to influence the work reported in this paper.

Acknowledgements

This research was funded by grant FPCI 28-0817 from the Facultad de Ciencias Sociales, Universidad de Chile. Research conducted on GNL Quintero 1 has benefited from the financial support of GNL Quintero S. A. VFA would like to thank T. Villaseñor for her helpful suggestions.

References

ÀRKA, 2008. Evaluación Arqueológica Subacuática Sitio GNL Quintero 1, Proyecto "Terminal de GNL en Quintero". Report commissioned by SGA Ltda, Comuna de Quintero, V Región.

ÀRKA, 2014. Informe Final Proyecto "Investigación Interdisciplinaria Sitio Paleontológico Sumergido GNL Quintero 1". Report commissioned by GNL Quintero, Comuna de Quintero, V Región. S.A. REF. INF11/2014.

Bailey, G., Galanidou, N., Peeters, H., Joens, H., Mennenga, M., 2020. The Archaeology of Europe's Drowned Landscapes, vol. 35. Coastal Research Library, Springer: Cham, ISBN 978-3-030-37367-2.

Benjamin, J., O'Leary, M., McDonald, J., Wiseman, C., McCarthy, J., Beckett, E., Morrison, P., Stankiewicz, F., Leach, J., Hacker, J., Baggaley, P., Jerbić, K., Fowler, M., Fairweather, J., Jeffries, P., Ulm, S., Bailey, G., 2020. Aboriginal artefacts on the continental shelf reveal ancient drowned cultural landscapes in northwest Australia. PloS One 15 (7), e0233912. https://doi.org/10.1371/journal.pone.0233912.

Bentley, M.J., Hodgson, D.A., Smith, J.A., O Cofaigh, C., Domack, E.W., Larter, R.D., Roberts, S.J., Brachfeld, S., Leventer, A., Hjort, C., Hillenbrand, C.-D., Evans, J., 2009. Mechanisms of Holocene palaeoenvironmental change in the antarctic peninsula region. Holocene 19, 51–69.

Brown, E.T., Johnson, T.C., Scholz, C.A., Cohen, A.S., King, J.W., 2007. Abrupt change in tropical African climate linked to the bipolar seesaw over the past 55,000 years. Geophys. Res. Lett. 34, L20702.

Brumfitt, I.M., Chinsamy, A., Compton, J.S., 2013. Depositional environment and bone diagenesis of the mio/pliocene Langebaanweg bonebed, South Africa. S. Afr. J. Geol. 116.2, 241–258. https://doi.org/10.2113/gssajg.116.2.241.

Carabias, D., Cartajena, I., Simonetti, R., López, P., Morales, C., Ortega, C., 2014. Submerged paleolandscapes: site GNL Quintero 1 (GNLQ1) and the first evidence from the Pacific coast of south America. In: Evans, A., Flatman, J., Flemming, N. (Eds.), Prehistoric Archaeology on the Continental Shelf. A Global Review. Springer, New York, pp. 131–149.

Carabias, D., Flores-Aqueveque, V., Simonetti, R., Cartajena, I., Ortega, C., Fernández, R., 2020. Factors Affecting Preservation and Identification of Submerged Paleolandscapes on the Pacific Coast of South America: Geoarchaeological Research Strategies for Site GNL Quintero 1, Central Chile (in preparation).

Carrillo-Briceño, J.D., Gonzalez-Barba, G., Landaeta, M.F., Nielsen, S.N., 2013. Condrictios fósiles del Plioceno superior de la Formación Horcón, Región de Valparaíso, Chile central. Rev. Chil. Hist. Nat. 86 (2), 191–206.

Cartajena, I., López, P., Carabias, D., Morales, C., Vargas, G., Ortega, C., 2013. First evidence of an underwater Final Pleistocene terrestrial extinct faunal bone assemblage from Central Chile (South America): taxonomic and taphonomic analyses. Quat. Int. 305, 45–55. https://doi.org/10.1016/j.quaint.2012.12.041.

Cartajena, I., López, P., Carabias, D., Pavez, J., Letelier, D., Simonetti, R., Morales, C., 2020. High-resolution digital recording techniques and taphonomic trajectories: multi-image photogrammetry applied to a drowned Late Pleistocene site in Central Chile (32°S). In: Rodrigues, J.A., Traviglia, A. (Eds.), Proceedings of the 6th International Congress on Underwater Archaeology (IKUWA6), ISBN 9781784916428, pp. 350–358.

Cartajena, I., Celis, F., Flores-Aqueveque, V., Pavez, J., Carabias, D., Simonetti, R., Arancibia, M.J., 2021. Mineral species and formation processes: Raman spectroscopic and microscopic analysis of stains from a late Pleistocene continental faunal bone assemblage, central Chile. Geoarchaeology 1–15. https://doi.org/10.1002/gea.21847.

Chatters, J.C., Rissolo, D., Arroyo-Cabrales, J., Stafford, T.W., Kemp, B.M., Alvarez, A., Nava Blank, A., Beddows, P.A., Reinhardt, E., Kovacs, S., Collins, S., Morell-Hart, S., Chávez Arce, R., Bird, S., Attolini Smithers, F., Luna Erreguerena, P., 2017. Hoyo negro: tapping the paleoanthropological and paleoecological potential of a deeply submerged underground chamber on the yucatan peninsula, Mexico. In: Campbell, P.B. (Ed.), The Archaeology of Underwater Caves. Highfield Press Southampton, UK, pp. 119–129.

Cherkinsky, A., 2009. Can we get a good radiocarbon age from "bad bone"? Determining the reliability of radiocarbon age from bioapatite. Radiocarbon 51, 647–655.

Colombera, L., Mountney, N.P., 2019. The lithofacies organization of fluvial channel deposits: a meta-analysis of modern rivers. Sediment. Geol. 383, 16–40.

Davison, W., 1993. Iron and manganese in lakes. Earth Sci. Rev. 34, 119–163.

Del Valle, F., Marquardt, C., Elgueta, S., Valdivia, D., 2017. Seismic Influence in the Quaternary Uplift of the Central Chile Coastal Margin, Preliminary Results. American Geophysical Union, Fall Meeting, New Orleans. Abstract #G53A-0759, 2017, December 11-15.

Del Valle, F., Marquardt, C., Valdivia, D., Elgueta, S., Yañez, G., 2018. Tasa de alzamiento neotectónico del margen costero chileno entre Los Vilos y Santo Domingo. In: Charrier, R. (Ed.), Actas del XV Congreso Geológico Chileno. Geociencias hacia la Comunidad. Universidad de Concepción, Chile, pp. 1303–1305.

Di Castri, F., Hajek, E., 1976. Bioclimatología de Chile. Editorial Universidad Católica de Chile, Santiago, p. 129.

Dunbar, J., 2012. The Search for Paleoindian Contexts in Florida and the Adjacent Southeast. Ph.D. Dissertation, Department of Anthropology Florida State University. Florida State University Libraries, Electronic Theses.

Dura, T., Cisternas, M., Horton, B.P., Ely, L.L., Nelson, A.R., Wesson, R.L., Pilarczyk, J.E., 2015. Coastal evidence for Holocene subduction-zone earthquakes and tsunamis in central Chile. Quat. Sci. Rev. 113, 93–111.

Folk, R.L., Ward, W.C., 1957. Brazos River bar: a study in the significance of grain size parameters. J. Sediment. Petrol. 27, 3–26.

Garreaud, R.D., Vuille, M., Compagnucci, R., Marengo, J., 2008. Present-day south American climate. Palaeogeogr. Palaeoclimatol. Palaeoecol. 281 (3–4), 180–195. https://doi.org/10.1016/j.palaeo.2007.10.032.

Garrison, E.G., Cook Hale, J., Cameron, C.S., Smith, E., 2016. The archeology, sedimentology and paleontology of Gray's Reef National Marine Sanctuary and nearby hard bottom reefs along the midcontinental shelf of the Georgia Bight. J. Archaeol. Sci. Rep. 5, 240–262. https://doi.org/10.1016/j.jasrep.2015.11.009.

Gibling, M.R., 2006. Width and thickness of fluvial channel bodies and valley fills in the geological record: a literature compilation and classification. J. Sediment. Res. 76 (5), 731–770.

Ginocchio, R., Carvallo, G., Toro, I., Bustamante, E., Silva, Y., Sepulveda, N., 2004. Micro-spatial variation of soil metal pollution and plant recruitment near a copper smelter in Central Chile. Environ. Pollut. 127, 343–352.

González, S., Ite, R., 1992. Acumulación metálica en suelos del área bajo influencia de las chimeneas industriales de Ventanas (Provincia de Valparaíso, V Región). Agric. Tec. (Santiago) 50, 214–219.

González, I., Neaman, A., Rubio, P., Cortés, A., 2014. Spatial distribution of copper and pH in soils affected by intensive industrial activities in Puchuncaví and Quintero, central Chile. J. Soil Sci. Plant Nutr. 14 (4), 943–953.

Halligan, J., Waters, M., Perrotti, A., Owens, I., Feinberg, J., Bourne, M., Fenerty, B., Winsborough, B., Carlson, D., Fisher, D., Stafford, T., Dunbar, J., 2016. Pre-Clovis occupation 14,550 years ago at the Page Ladson site, Florida, and the peopling of the Americas. Sci. Adv. 2 (5), e1600375 https://doi.org/10.1126/sciadv.1600375.

Hedrick, J.B., 2000. Zirconium and Hafnium. US Geological Survey, Mineral Information.

Hogg, A., Heaton, T., Hua, Q., Palmer, J., Turney, C., Southon, J., Bayliss, A., Blackwell, P., Boswijk, G., Ramsey, B., Pearson, C., Petchey, F., Reimer, P., Reimer, R., Wacker, L., 2020. SHCal20 southern hemisphere calibration, 0–55,000 Years cal BP. Radiocarbon 62 (4), 759–778. https://doi.org/10.1017/RDC.2020.59.

Isla, F., 1989. Holocene sea-level fluctuation in the southern hemisphere. Quat. Sci. Rev. 8, 359–368.

Kaiser, J., Schefuß, E., Lamy, F., Mohtadi, M., Hebbeln, D., 2008. Glacial to Holocene changes in sea surface temperature and coastal vegetation in north central Chile: high versus low latitude forcing. Quat. Sci. Rev. 27, 2064–2075.

Kendrick, D.C., 2006. Stratigraphy and sedimentation. In: Webb, S.D. (Ed.), First Floridians and Last Mastodons: the Page-Ladson Site in the Aucilla River. Springer, Dordrecht. https://doi.org/10.1007/978-1-4020-4694-0_3.

Kristensen, E., 2000. Organic matter diagenesis at the oxic/anoxic interface in coastal marine sediments, with emphasis on the role of burrowing animals. Hydrobiologia 426, 1–24.

Kylander, M.E., Ampel, L., Wohlfarth, B., Veres, D., 2011. High-resolution X-ray fluorescence core scanning analysis of Les Echets (France) sedimentary sequence: new insights from chemical proxies. J. Quat. Sci. 26, 109–117.

Lambeck, K., Roubya, H., Purcella, A., Sunc, Y., Sambridge, M., 2014. sea Level and global ice volumes from the last glacial maximum to the Holocene. Proc. Natl. Acad. Sci. Unit. States Am. 111 (43), 15296–15303. https://doi.org/10.1073/pnas.1411762111.

López, P., Labarca, R., Núñez, L., 2004. Nivel Quereo I: una Discusión Acerca del Poblamiento Temprano en la Provincia del Choapa: Revista. Werken 5, 15–20.

López, P., Cartajena, I., Olivares, G., López, O., Carabias, D., Morales, C., 2012. Aplicación de Microscopio electrónico de Barrido (MEB) y espectroscopia de Energía dispersiva (EDS). In: Acosta, A., Loponte, D., Muscio, L. (Eds.), para distinguir alteraciones térmicas en restos osteofaunísticos de un sitio sumergido del Pleistoceno final de la costa de Chile central. En Temas de Arqueología, Estudios Tafonómicos y Zooarqueológicos (II). Instituto Nacional de Antropología y Pensamiento Latinoamericano, Buenos Aires, pp. 25–44.

López, P., Cartajena, I., Carabias, D., Morales, C., Letelier, D., Flores, V., 2016. Terrestrial and maritime taphonomy: differential effects on spatial distribution of a Late Pleistocene continental drowned faunal bone assemblage from the Pacific coast of Chile. Archaeol. Anthropol. Sci. 8, 277–290. https://doi.org/10.1007/s12520-015-0275-y.

López, P., Cartajena, I., Carabias, D., Prevosti, F., Maldonado, A., Flores-Aqueveque, V., 2018. Reconstructing drowned terrestrial landscapes. Isotopic paleoecology of a late Pleistocene extinct faunal assemblage: site GNL Quintero 1 (GNLQ1) (32° S, Central Chile). Quat. Int. 463 (A) https://doi.org/10.1016/j.quaint.2016.08.017, 153-150.

Mackenzie, L., Heijnis, H., Gadd, P., Moss, P., Shulmeister, J., 2017. Geochemical investigation of the South Wellesley Island wetlands: insight into wetland development during the Holocene in tropical northern Australia. Holocene 27 (4), 566–578. https://doi.org/10.1177/0959683616670219.

Martinod, J., Regard, V., Riquelme, R., Aguilar, G., Guillaume, B., Carretier, S., Cortes Aranda, J., Leanni, L., Hérail, G., 2016. Pleistocene uplift, climate, and morphological segmentation of the northern Chile coasts (24°S-32°S): insights from cosmogenic 10Be dating of paleoshorelines. Geomorphology 274, 78–91.

Melnick, D., 2016. Rise of the central Andean coast by earthquakes straddling the Moho. Nat. Geosci. 9, 401–407.

Méndez, C., Seguel, R., Nuevo-Delaunay, A., Murillo, I., López, P., Jackson, D., Maldonado, A., 2020. Depositional contexts and new age controls for terminal-pleistocene megafauna in north-central Chile (31°50′S). PaleoAmerica. https://doi.org/10.1080/20555563.2020.1733384.

Moreno, A., Giralt, S., Valero-Garcés, B., Sáez, A., Bao, R., Prego, R., Pueyo, J.J., González-Sampériz, P., Taberner, C., 2007. A 14 kyr record of the tropical Andes: the Lago Chungará sequence (18°S, northern Chilean Altiplano). Quat. Int. 161, 4–21.

Munsell Color, 2009. Munsell Soil-Color Charts. Munsell Color, Grand Rapids.

Naeher, S., Gilli, A., North, R.P., Hamann, Y., Schubert, C.J., 2013. Tracing bottom water oxygenation with sedimentary Mn/Fe ratios in Lake Zurich, Switzerland. Chem. Geol. 352, 125–133.

Núñez, L., Varela, J., Casamiquela, R., Villagrán, C., 1994. Reconstrucción Multidisciplinaria de la Ocupación Prehistórica de Quereo, Centro de Chile. Lat. Am. Antiq. 5 (2), 99–118.

Olivares, G., Gallardo, L., Langner, J., Aarhus, B., 2002. Regional dispersion of oxidized sulfur in Central Chile. Atmos. Environ. 36, 3819–3828.

O'Shea, J., 2021. Submerged prehistory in the Americas: methods, approaches and results. J. I. Coast Archaeol. 16 (1), 1–4. https://doi.org/10.1080/15564894.2021.1879973.

Parra, S., Bravo, M.A., Quiroz, W., Moreno, T., Karanasiou, A., Font, O., Vidal, V., Cereceda, F., 2014. Distribution of trace elements in particle size fractions for contaminated soils by a copper smelting from different zones of the Puchuncaví Valley (Chile). Chemosphere 111, 513–521. https://doi.org/10.1016/j.chemosphere.2014.03.127.

Parra, S., Bravo, M.A., Quiroz, W., Querol, X., Paipa, C., 2015. Distribution and pollution assessment of trace elements in marine sediments in the Quintero Bay (Chile). Mar. Pollut. Bull. 99 (1–2), 256–263.

Quintana, J.M., Aceituno, P., 2012. Changes in the rainfall regime along the extratropical west coast of South America (Chile): 30–43° S. Atmósfera 25, 1–22.

Quinton, J.N., Catt, J.A., Hess, T.M., 2001. The selective removal of phosphorus from soil: is event size important? J. Environ. Qual. 30, 538–545.

Reddy, K.R., Kadlec, R.H., Flaig, E., Gale, P.M., 1999. Phosphorus assimilation in streams and wetlands: a review. Crit. Rev. Environ. Sci. Technol. 29, 83–146.

Rivano, S., Sepúlveda, P., Boric, R., Espiñeira, D., 1993. Geología de la Hoja Quillota-Portillo, V Región, escala 1:250.000. Servicio Nacional de Geología y Minería, Santiago.

Saillard, M., Audin, L., Rousset, B., Avouac, J.-P., Chlieh, M., Hall, S.R., Husson, L., Farber, D.L., 2017. From the seismic cycle to long-term deformation: linking seismic coupling and Quaternary coastal geomorphology along the Andean megathrust. Tectonics 36. https://doi.org/10.1002/2016TC004156.

Semeniuk, V., Semeniuk, C.A., 2004. Sedimentary fill of basin wetlands, central Swan Coastal Plain, southwestern Australia. Part 1: sediment particles, typical sediments, and classification of depositional systems. J. Roy. Soc. West Aust. 87, 139–186.

Smith, D.E., Harrison, S., Firth, C.R., Jordan, J.T., 2011. The early Holocene sea level rise. Quat. Sci. Rev. 30, 1846–1860.

Syers, J.K., Walker, T.W., 1969. Fractionation of phosphorus in two cultivated soils and particle size separates. Soil Sci. 108, 283–289.

Thomas, H., 1958. Geología de la Cordillera de la costa entre el Valle de La Ligua y La Cuesta de Barriga, vol. 2. Boletín del Instituto de Investigaciones Geológicas, Boletín (Chile), p. 86.

Toggweiler, J.R., 2009. Climate change: shifting westerlies. Science 323, 1434. https://doi.org/10.1126/science.1169823.

Vargas, G., Pantoja, S., Rutllant, J.A., Lange, C.B., Ortlieb, L., 2007. Enhancement of coastal upwelling and interdecadal ENSO-like variability in the Peru-Chile Current since late 19th century. Geophys. Res. Lett. 34, L13607. https://doi.org/10.1029/2006GL028812.

Vargas, G., Ortega, C., 2008. Contexto geomorfológico y análisis sedimentológico preliminar de Muestras de la Bahía Quintero, V región. Proyecto terminal GNL Quintero. ARKA Consultores 2008, Evaluación Arqueológica Subacuática Sitio GNL Quintero 1. September 2008.

Veit, H., Preusser, F., Trauerstein, M., 2015. The Southern Westerlies in Central Chile during the two last glacial cycles as documented by coastal aeolian sand deposits and intercalating palaeosols. Catena 134, 30–40.

Villa-Martínez, R., Villagrán, C., 1997. Historia de la Vegetación de Bosques Pantanosos de la Costa de Chile Central Durante el Holoceno Medio y Tardío. Rev. Chil. Hist. Nat. 70, 391–401.

Villagrán, C., Varela, J., 1990. Palynological evidence for increased aridity on the central Chile coast during the Holocene. Quat. Res. 34, 198–207.

Wennrich, V., Minyuk, P.S., Borkhodoev, V., Francke, A., Ritter, B., Nowaczyk, N.R., Sauerbrey, M.A., Brigham-Grette, J., Melles, M., 2014. Pliocene to Pleistocene climate and environmental history of Lake El'gygytgyn, Far East Russian Arctic, based on high-resolution inorganic geochemistry data. Clim. Past 10, 1381–1399.

Werz, B.E., Flemming, N.C., 2001. Discovery in Table Bay of the oldest handaxes yet found underwater demonstrates preservation of hominid artefacts on the continental shelf. South Afr. J. Sci. 97 (5), 183–185.

Wuana, R.A., Okieimen, F.E., 2011. Heavy metals in contaminated soils: a review of sources, chemistry, risks and best available strategies for remediation. ISRN Ecol. 1–20.